HHS Public Access

Author manuscript

Nat Commun. Author manuscript; available in PMC 2014 May 18.

Published in final edited form as:

Nat Commun. 2013 ; 4: 2805. doi:10.1038/ncomms3805.

Orai1-dependent Calcium Entry Promotes Skeletal Muscle Growth and Limits Fatigue

Lan Wei-LaPierre[1], **Ellie M. Carrell**[1], **Simona Boncompagni**[2], **Feliciano Protasi**[2], and **Robert T. Dirksen**[1,*]

[1]Department of Physiology and Pharmacology, University of Rochester, 601 Elmwood Avenue, Rochester, NY, 14642

[2]CeSI - Center for Research on Ageing & DNI - Dept. of Neuroscience and Imaging; University G. d'Annunzio, Chieti, I-66013, Italy

Abstract

Store-operated Ca^{2+} entry (SOCE) in skeletal muscle involves signaling between stromal interaction molecule 1 (STIM1) in the sarcoplasmic reticulum and Ca^{2+} selective Orai1 channels in the sarcolemma. Here we generate transgenic mice with muscle-specific expression of dominant-negative Orai1 (dnOrai1) and demonstrate that Orai1-dependent SOCE promotes growth and limits fatigue in adult skeletal muscle. dnOrai1 mice lack SOCE specifically in muscle but are fertile and thrive well into adulthood. Although muscle ultrastructure, excitation-contraction coupling fiber type, and expression of other Ca^{2+} regulatory proteins are unaltered, dnOrai1 mice exhibit reduced body weight, muscle mass, and fiber cross-sectional area. Importantly, during intense repetitive activity, dnOrai1 mice display increased susceptibility to fatigue at the single fibre, excised muscle, and whole animal levels. We further show that STIM1 and Orai1 proteins colocalise within the triad junction but do not exist in a preassembled context. These results show that Orai1-dependent SOCE has an important physiological role in muscles of adult mice.

INTRODUCTION

Store-operated Ca^{2+} entry (SOCE) is activated by depletion of intracellular Ca^{2+} stores[1]. In non-excitable cells, SOCE is coordinated by stromal interacting molecule 1 (STIM1) serving as an ER Ca^{2+} sensor[2-4] that activates Ca^{2+}-selective Orai1 channels in the plasma membrane[5, 6]. Specifically, store depletion results in Ca^{2+} unbinding from the luminal EF hand domain of STIM1, which induces STIM1 aggregation and translocation to adjacent

*Corresponding author: Robert T. Dirksen Robert_Dirksen@URMC.Rochester.edu.

AUTHOR CONTRIBUTIONS

R.T.D. and L.W.L. designed research; S.B., E.M.C., and L.W.L. performed experiments and analysed data; R.T.D., L.W.L., and F.P. wrote the manuscript.

CONFLICT OF INTEREST

The authors declare no conflict of interest.

ER-plasma membrane junctions. Within these junctions, STIM1 aggregates interact with Orai1 to activate the channel and promote Ca^{2+} influx[7-10].

SOCE in skeletal myotubes exhibits a similar biophysical, pharmacological, and molecular signature as that observed in non-excitable cells. SOCE in myotubes is activated by depletion of sarcoplasmic reticulum (SR) Ca^{2+} stores and is inhibited by multiple SOCE inhibitors including lanthanide, BTP-2, 2-APB, and SK&F 96365[11-14]. SOCE in myotubes depends on STIM1-Orai1 coupling as it is abolished by both STIM1 knock-down and expression of dominant-negative Orai1 (E106Q)[12, 14, 15]. SOCE is also absent in myotubes derived from mice with global[13] or skeletal muscle-specific[11] deletion of STIM1. Finally, voltage clamp studies[14] indicate that the SOCE channel current in myotubes exhibits similar biophysical, pharmacological and molecular properties as that observed in T-lymphocytes[16, 17].

While SOCE in muscle has been linked to Ca^{2+} store repletion[18], fatigue[19, 20], NFAT transactivation[13, 21] and muscle differentiation[11, 13, 22], the precise physiological role(s) of STIM1-Orai1 coupling and Orai1-dependent Ca^{2+} entry in adult skeletal muscle remains unclear. Rosenberg and colleagues reported that global and muscle-specific STIM1 ablation results in a profound reduction in muscle mass, a severe myopathy, and neonatal lethality[11, 13]. However, STIM1 is a multi-purpose stress transducer activated by diverse stimuli (depletion, oxidation, temperature, hypoxia, and acidification) that regulates multiple targets including channels (Orai1, TrpC, ARC, and Cav1.2), pumps/exchangers (SERCA, PMCA, Na/Ca exchanger), adaptor proteins (POST), ER chaperones (calnexin and ERp57), signaling enzymes (adenylate cyclase isoform 8) and ER stress/remodeling proteins (microtubule protein EB1)[23]. Thus, the specific role of STIM1-Orai1 coupling in the survival and complex muscle phenotypes of STIM1 knockout mice is unclear.

To determine the role of Orai1-dependent Ca^{2+} entry in skeletal muscle structure and function, we generated transgenic mice with muscle-specific expression of dominant negative Orai1 (dnOrai1 mice). Remarkably, unlike STIM1 knockout mice, dnOrai1 mice are viable, fertile and live a normal lifespan. Thus, dnOrai1 transgenic mice enabled determination of the specific role of Orai1-dependent Ca^{2+} entry in skeletal muscle growth, development, and performance in adult animals.

RESULTS

STIM1 and Orai1 do not form preassembled triad complexes

While STIM1-Orai1 coupling underlies SOCE in myotubes, this has not been rigorously determined in fully-differentiated adult skeletal muscle fibres. Using immunocytochemical studies in single mouse *flexor digitorum brevis* (FDB) fibres from adult mice, Orai1 exhibited a double-row pattern of fluorescence that co-localised with the ryanodine receptor (Fig. 1a), confirming the presence of Orai1 within the triad junction. STIM1 fluorescence was observed throughout the I band region, flanking discrete Z-disk localization α-actinin, though also significantly enriched with RyR1 in the triad (Fig. 1b,c). Co-localisation of STIM1 and Orai1 in the triad of resting muscle fibres is consistent with a uniquely extremely rapid (e.g. tens of ms) and efficient SOCE activation upon SR Ca^{2+} store

depletion in muscle[14, 24-26]. In order to support such rapid activation, STIM1 and Orai1 have been proposed to be closely associated or even form preassembled complexes that are directly activated upon store depletion [25, 27]. This hypothesis was tested using bi-molecular fluorescence complementation (BiFC)[28-30] to determine if junctional STIM1 and Orai1 proteins form preassembled SOCE channel complexes in fibers with fully replete SR Ca^{2+} stores. FDB muscles were electroporated with cDNAs encoding cherry-STIM1-$N_{(1-158)}$YFP and cherry-Orai1-$C_{(159-283)}$YFP. While expressing fibres lacked basal YFP fluorescence, robust junctional YFP fluorescence was observed following thapsigargin (TG)-induced store depletion (Fig. 1d,e). Thus, while STIM1 and Orai1 co-localise in the triad, they do not form preassembled STIM1-Orai1 complexes in the absence of SR store depletion.

Characterization of SOCE in adult skeletal muscle fibres

We used Mn^{2+} quench of fura-2 fluorescence[12] to examine the molecular determinants and pharmacological signature of SOCE in FDB fibres from adult mice. While fura-2 emission was unaltered during application of extracellular Mn^{2+} in non-depleted fibres (Fig. 2a), a significant increase in fura-2 quench rate was observed in TG-treated fibres (Fig. 2b), consistent with robust SOCE activation. Mn^{2+} quench in store-depleted fibers was inhibited by addition of either 0.2 mM $LaCl_3$ or 10 μM BTP-2 (Fig. 2c-d). To assess the importance of Orai1 in this store-dependent entry, cherry-tagged dominant negative Orai1E108Q was transiently expressed by electroporation in FDB muscles of adult mice. TG-pretreated, E108Q-expressing fibres lacked a significant change in fura-2 quench upon addition of extracellular Mn^{2+} (Fig. 2e). Electroporation of FDB muscles with a mixture of four STIM1-specific siRNAs, but not negative control siRNAs (Supplementary Table S1), markedly reduced expression of both short (average ± s.e.m.: 62±12%) and long (average ± s.e.m.: 80±5%) STIM1 isoforms (Supplementary Fig. S1). STIM1 knockdown abolished Mn^{2+} quench in FDB fibers following store depletion (Fig. 2f), while no effect was observed for negative control siRNAs (Fig. 2g). Average (±s.e.m.) values for the maximal rate of Mn^{2+} quench for the conditions shown in Fig. 1a-g are summarized in Fig. 1h. These results demonstrate that SOCE in adult skeletal muscle requires STIM1-Orai1 coupling and that this process is abolished by expression of dominant negative Orai1.

Effect of SOCE on Ca^{2+} transients during tetanic stimulation

Since SR Ca^{2+} stores in FDB fibres are significantly reduced during a single high frequency stimulation train[31], we determined the effect of inhibiting SOCE on myoplasmic Ca^{2+} transients elicited by multiple repetitive, high frequency tetanic stimulation trains (Fig. 3). Myoplasmic Ca^{2+} transients were monitored in single FDB fibres using mag-fluo-4, a rapid, low affinity Ca^{2+} dye that maximizes resolution of Ca^{2+} transient magnitude and kinetics[32]. Mag-fluo-4-loaded fibres were stimulated for 60 consecutive tetanic trains (500 ms, every 2.5 s, at 50 Hz, 60 times). Ca^{2+} transient magnitude during each tetani and the integral of the decaying phase of the Ca^{2+} transient ("tail Ca^{2+} transient integral") following termination of each train were quantified (Supplementary Fig. S2a).

In FDB fibres perfused with control Ringer's solution, peak tetanic Ca^{2+} transient amplitude decreased progressively from the first train, reaching approximately 50% by the 60th train (Fig. 3a). In the presence of 0.2 mM $LaCl_3$ plus 0.5 mM $CdCl_2$ (La/Cd), the amplitude of the

first tetanic Ca^{2+} transient was not significantly different from that observed in control, consistent with the independence of skeletal muscle excitation-contraction (EC) coupling on Ca^{2+} entry. However, the decrement in tetanic Ca^{2+} transient magnitude was significantly greater by the 30th train, and even more so by the 60th train, in the presence of La/Cd (Fig. 2a and Supplementary Fig. S2b). As a result, a clear sustained phase of Ca^{2+} transient amplitude was observed between T10 and T40 under control conditions (−4.3±2.8%, average ± s.e.m.:) that was reduced ~7-fold in the presence of La/Cd (−29.9±2.8%) (Fig. 3b). Similarly, the tail Ca^{2+} transient integral, which reflects a balance between Ca^{2+} influx and removal and increased (+10.2±9.6%, average ± s.e.m.:) between T40 and T10 in control (T40-T10), was reduced in the presence of La/Cd (−21.7±6.2%) (Fig. 3c-d).

Since La/Cd blocks multiple forms of Ca^{2+} entry, effects of more targeted SOCE interventions were also determined. A similar accelerated reduction in peak Ca^{2+} transient amplitude (Fig. 3a-b) and tail integral (Fig. 3c-d) during repetitive tetanic stimulation was observed following addition of SOCE channel inhibitors SK&F-96365 (30 μM) and BTP-2 (10 μM). Most importantly, a faster decay in peak Ca^{2+} transient amplitude (Fig. 3e-f) and tail Ca^{2+} transient integral (Fig. 3g-h) was also observed in FDB fibres following STIM1 knockdown (STIM KD, but not for control siRNA) and transient expression of Orai1E108Q mutant. The results in Fig. 3 indicate that SOCE plays an important role in maintaining Ca^{2+} transient amplitude during repetitive, high frequency tetanic stimulation.

Characterization of muscle-specific dnOrai1 transgenic mice

SOCE is abolished in myotubes[12] and FDB fibers following transient expression of Orai1E108Q (Fig. 2e and h). Therefore, in order to investigate the role of Orai1-dependent Ca^{2+} entry in adult skeletal muscle, we generated muscle-specific dnOrai1 (E108Q) transgenic mice (Fig. 4a; see Methods). Several transgenic lines exhibiting either low (line 102), medium (line 5) or high but variable (line 86) dnOrai1 expression were generated (Fig. 4b). Expression of the dnOrai1 protein assessed using an anti-HA antibody was highly skeletal muscle specific, with no detectable expression in heart, spleen, liver, lung, or kidney (Fig. 4c). The dnOrai1 protein was partially glycosylated since the doublet band observed on western blot was consolidated to a single band following de-glycosylation with PNGaseF (Fig. 4c). Immunocytochemistry of FDB fibres from line 5 mice using an anti-HA antibody showed a double-rowed striated pattern that co-localised with STIM1 fluorescence (Fig. 4d), similar to that observed for endogenous Orai1 (Fig. 1a). Importantly, FDB fibers obtained from both line 86 (Fig. 4e-f) and line 5 (Fig. 4f) mice lacked SOCE as assessed by Mn^{2+} quench.

Unlike that observed following global or muscle-specific STIM1 ablation[11, 13], line 5 muscle-specific dnOrai1 transgenic mice were born at normal Mendelian ratios, thrived into adulthood, and exhibited normal activity and fertility during the course of study up to 10 months of age. Similar to STIM1 knockout mice, line 5 dnOrai1 mice exhibited a significant reduction in whole-body mass at birth compared to WT littermates, which persisted throughout postnatal development and into adulthood (Fig. 5a). Muscle mass of *tibialis anterior* (TA), *extensor digitorum longus* (EDL), and *soleus* (SOL) muscles were all significantly reduced (~20-30%) in line 5 dnOrai1 mice compared to WT littermates (Fig.

5b). Analysis of muscle cross sectional area (CSA) by dystrophin immunolabeling revealed a significant reduction (~33%) in average fibre CSA in TA muscles of line 5 dnOrai1 mice (Fig. 5c-d). Nevertheless, hematoxylin and eosin (H&E) staining of TA muscle sections showed no evidence of muscle damage, degeneration, central nucleation, or infiltration of inflammatory fibres from line 5 dnOrai1 mice (Fig. 5c, bottom). In addition, myosin heavy chain analyses revealed no change in the proportion of type I, IIa, IIx, or IIb fibres in TA, EDL, SOL and FDB muscles (Fig. 5e-f). Using electron microscopy (EM), the ultrastructure, myofibril spacing, and disposition of SR, transverse tubules, triads, and mitochondria in EDL and FDB fibers from line 5 dnOrai1 mice were indistinguishable from WT (see Fig. 6 for additional details). Only a few fibres from line 5 dnOrai1 mice (3/63) exhibited minor structural defects (limited regions of Z-line streaming or a few swollen mitochondria).

Western blot analysis using an Orai1-specific antibody showed no change in endogenous Orai1 expression in TA muscles of dnOrai1 mice (Supplementary Fig. S3a). Expression of STIM1 (Supplementary Fig. S3b) and other proteins involved in Ca^{2+} homeostasis (i.e. Sarco/Endoplasmic Ca^{2+} ATPase 1, RyR1, calsequestrin type 1, and dihydropyridine receptor α1-subunit; Supplementary Fig. S4) were also unaltered in TA muscles of dnOrai1 mice. Consistent with this, the magnitude and decay kinetics of electrically-evoked twitch Ca^{2+} release was not different in single FDB fibres from adult WT and dnOrai1 mice (Supplementary Fig. S5a-c). However, total Ca^{2+} store content assessed using a rapid Ca^{2+} store release cocktail[33] was significantly reduced ($p<0.01$, *Student's t*-test) in FDB fibres from dnOrai1 mice (fura2FF ΔRatio was 0.36±0.03, average ± s.e.m. n-11 and 0.17±0.05, n=6 for WT and dnOrai1, respectively; Supplementary Fig. S5d-e).

dnOrai1 mice exhibit increased susceptibility to fatigue

As muscle-specific dnOrai1 mice thrive into adulthood and lack SOCE in skeletal muscle (Fig. 4e-f), these mice provide a unique opportunity to determine the physiological role of Orai1-dependent SOCE in adult muscle. As an initial test of the functional impact of loss of SOCE in muscle, we compared *ex vivo* muscle contractility of EDL muscles isolated from 4-6 month old WT and line 5 dnOrai1 mice. The magnitude and kinetics of EDL twitch contraction were not different between WT and dnOrai1 (Fig. 7a, left traces), consistent with the normal fiber type distribution, ultrastructure, and EC coupling in muscles from dnOrai1 mice. However, a modest reduction in peak muscle specific force was observed in EDL muscles from dnOrai1 mice at stimulation frequencies ≥100 Hz (Fig. 7ab). EDL muscles from dnOrai1 mice also exhibited a reduced ability to maintain contractile force at high frequencies during each 500 ms stimulation (Fig. 7a, grey traces and 7c), consistent with an increase in EDL fatigability during intense stimulation. Moreover, the magnitude of force decay during a prolonged tetanus (150Hz, 2s) was increased in EDL muscles from dnOrai1 mice (Fig. 7d-e).

We next compared the ability of muscles from dnOrai1 mice to produce sustained Ca^{2+} release and force production during repetitive high frequency tetanic stimulation (Fig. 8a-d). Single FDB fibres from WT and dnOrai1 mice were subjected to the same repetitive tetanic stimulation train used for the experiments shown in Fig. 3 (50 Hz, 500 ms, every 2.5 s, 60

times). Consistent with results obtained with SOCE channel inhibitors, STIM1 KD, and Orai1E108Q expression, peak tetanic Ca^{2+} transient decline was accelerated in FDB fibres from dnOrai1 mice (Fig. 8a). Peak Ca^{2+} transient amplitude decreased 47.0±7.3% (average ± s.e.m.) from T5 to T40 in fibres from dnOrai1 mice, in contrast to only 15.6±9.6% for fibres from WT mice (Fig. 8b). A similar accelerated decline in force production repetitive tetanic stimulation was also observed in EDL muscles from dnOrai1 mice (Fig. 8c), where tetanic force during the first 5 tetani decreased 14.6±2.7% (average ± s.e.m.) for dnOrai1 compared to only 7.4±1.6% for WT (Fig. 8d). A similar decrease in peak specific force and increased fatigability during repetitive stimulation were observed in EDL muscles from dnOrai1 line 86 mice (Supplementary Fig. S6) Together, these results are consistent with a significant contribution of SOCE to sustained Ca^{2+} release and force production during repetitive, high frequency stimulation.

Finally, dnOrai1 mice were used to assess the consequences of loss of SOCE function on muscle performance at the whole animal level. Age- (4-5 month old male) and sex-matched WT and line 5 dnOrai1 mice were evaluated using a prolonged Rota-Rod protocol designed to assess endurance. In this test, mice were placed on a motor driven Rota-Rod wheel and forced to walk on the rotating wheel for 2 h while the speed was increased modestly at regular intervals (see Methods). WT mice remained on the wheel with only a few falls during the first hour, with progressively more falls during the second hour. On the other hand, while initially performing equally well at the task, dnOrai1 mice exhibited a significant increase in the number of cumulative falls compared to WT mice at all times 30 minutes after initiation of the task (Fig. 8e and Supplementary Movie 1). Due to exhaustion, several dnOrai1 mice were unable to complete the entire 2 h protocol. Thus, only the cumulative number of falls during the first 60 min of the task is shown in Fig. 8e. As a second measure of fatigue, a separate group of WT and line 5 dnOrai1 mice were subjected to three consecutive days of acute treadmill running (see Methods). All WT and dnOrai1 mice completed the entire 1 kilometer run on each of three consecutive days. However, WT mice completed the task with limited rests and encouragement. On the other hand, after the first ~40 minutes of running, dnOrai1 mice exhibited a significant increase in the number of rests and required more encouragement to re-engage the treadmill and continue running (Fig. 8f and Supplementary Movie 2). Together, results from the Rota-Rod exhaustion and treadmill running tasks indicate that adult dnOrai1 mice exhibit a significantly increased susceptibility to muscle fatigue.

DISSCUSION

This study characterized the structural basis and physiological role of SOCE in adult skeletal muscle. Immunocytochemical results provide direct evidence for co-localisation of endogenous Orai1 and STIM1 in the triad junction and Mn^{2+} quench studies found that STIM1-Orai1 coupling is required for SOCE in adult skeletal muscle. This close disposition of STIM1 and Orai1 in existing SR-T-tubule triad junctions enables rapid SOCE activation since STIM1 and SR redistribution following store depletion is not required. However, results of BiFC experiments indicate that preformed STIM1-Orai1 complexes are not present in resting muscle fibres with fully replete SR Ca^{2+} stores and that store depletion is required to drive the formation of junctional Orai1-STIM1 complexes. FRET-based studies

will be required to further resolve the time course of junctional STIM1-Orai1 complex formation during SR Ca^{2+} store depletion.

The survival of muscle-specific dnOrai1 mice allowed us to assess the physiological role of Orai1-dependent SOCE in adult skeletal muscle. While line 5 dnOrai1 mice lack SOCE, these mice thrive into adulthood and exhibit normal muscle histology and fiber type distribution. Thus, Orai1-dependent SOCE is clearly not required for survival. However, as muscle mass and CSA are reduced in line 5 dnOrai1 mice, SOCE is required for normal muscle growth. While high expressing line 86 mice are fertile, live well into adulthood, and exhibit a similar reduction in muscle mass and CSA, some of these mice exhibit histopathological signs of myopathy including increased cell infiltration, central nucleation, and the development of kyphosis at advanced ages. The myopathic phenotypes observed in line 86 mice is unlikely due to loss of Orai1-dependent SOCE since they are not observed in line 5 mice that also lack SOCE. The reasons for the variable myopathic alterations observed in line 86 dnOrai1 mice is unclear but may involve off-target effects (e.g. inhibition of TrpC channels)[34] of the high level of dnOrai1 expression observed in some of these mice (Fig. 4b).

The role of SOCE in refilling SR Ca^{2+} stores in skeletal muscle is controversial. On the one hand, SR Ca^{2+} content was reported to be increased in FDB fibers from *mdx* mice[35] where Orai1[35,36] and STIM1[36] protein levels are up-regulated and SOCE is enhanced, while SR Ca^{2+} store content is reduced in muscle-specific STIM1 knockout mice that lack SOCE.[11] However, since other critical Ca^{2+} handling proteins (e.g. SERCA, TrpC3/6, NCX3) are also altered in these models,[11,35] the specific role of STIM1-Orai1 coupling in store refilling remains unclear. In addition, Launikonis and colleagues reported that in spite of changes in STIM1 and Orai1 expression in *mdx* muscle, SR Ca^{2+} content was unaltered in mechanically skinned EDL muscle fibers,[36] and thus, concluded that SOCE has little or no role in refilling SR Ca^{2+} stores in skeletal muscle [25, 36, 37]. However, as SR reloading in mechanically skinned fibres may be different from that of intact fibres, the relevance of these results to Ca^{2+} store content in intact fibers under more physiological conditions is unclear. Our finding that resting Ca^{2+} store content was significantly reduced in intact single FDB fibres from dnOrai1 mice is consistent with Orai1-dependent Ca^{2+} entry playing a role in maintaining and refilling SR Ca^{2+} stores as it does in non-excitable cells. In addition, since no alterations in other major Ca^{2+} handling proteins were found in muscle from dnOrai1 mice (Supplementary Figure S4), our findings provide the strongest evidence to date that Orai1-dependent SOCE contributes to store refilling in skeletal muscle.

The reduction in total Ca^{2+} store content likely contributes to the reduced peak tetanic specific force and accelerated fatigue with repetitive high frequency stimulation. During repetitive tetanic stimulation of FDB fibres from WT mice, peak Ca^{2+} transient magnitude is maintained and Ca^{2+} transient tail integral is increased, both of which are reduced by SOCE inhibitors, STIM1 KD, and dnOrai1 expression. These findings indicate that repetitive tetanic stimulation promotes store depletion and activation of STIM1/Orai1-dependent SOCE needed to replenish SR Ca^{2+} stores and maintain Ca^{2+} release during subsequent tetani. Thus, SOCE plays an important role in sustaining Ca^{2+} release and contractile force during repetitive tetanic stimulation, consistent with that reported previously when SOCE

activity is reduced either pharmacologically[19] or in aging[38]. Our findings that adult dnOrai1 mice exhibit a marked increased susceptibility to exhaustion during prolonged Roto-Rod and treadmill exercise provide the strongest evidence to date that Orai1-dependent SOCE plays a key role in limiting muscle fatigue during strenuous exercise.

Muscle-specific dnOrai1 transgenic mice also provide insight into the role of Orai1-dependent SOCE in skeletal muscle development, specification, growth, and survival. As reported for muscle-specific STIM1 knockout mice[11], dnOrai1 mice exhibit similar reductions in body weight, muscle mass, and fibre CSA. Taken together, these findings demonstrate that STIM1-Orai1 signaling promotes muscle growth in both young and adult mice, presumably through activation of Ca^{2+}-dependent downstream signaling cascades[11]. However, STIM1 knockout mice also exhibit hypotonia, increased central nucleation, swollen mitochondria, and neonatal lethality[11, 13], none of which are observed in line 5 dnOrai1 mice. These additional phenotypes observed in STIM1 knockout mice, but not in line 5 dnOrai1 mice, likely reflect altered activity of one or more non-Orai1 STIM1 targets including TrpC/ARC/Ca_V channels, SERCA/PMCA/NCX pumps/exchangers, adaptor proteins, ER chaperones, second messenger enzymes, or ER stress/remodeling proteins[23].

In summary, we provide a comprehensive characterization of Orai1-dependent SOCE in adult skeletal muscle. SOCE in adult muscle depends on junctional STIM1-Orai1 coupling, which is important for both normal muscle growth and susceptibility to fatigue. Altered SOCE activity has been proposed to contribute to muscle dysfunction in various pathophysiological states of muscle including sarcopenia[38], muscular dystrophy[36], and malignant hyperthermia[39]. Muscle-specific dnOrai1 mice will provide a powerful model to assess the relative importance of Orai1-dependent SOCE in normal muscle physiology and how SOCE dysfunction contributes to these and other muscle pathologies.

METHODS

In vivo electroporation of FDB muscles

All experiments were approved by the University of Rochester Committee on Animal Recourses. 4-6 months old male and female WT C57Bl6 mice were anesthetized by intraperitoneal injection of 100 mg/kg ketamine, 10 mg/kg xylazine, and 3 mg/kg acepromazine. Hindlimb footpads of anesthetized mice were then injected with bovine hyaluronidase (10 μl, 0.4U/ μl). One hour later, hindlimb footpads were subcutaneously injected with either cherry-tagged Orai1cDNA construct (20 μg in 71 mM NaCl), STIM1-specific siRNAs (Dharmacon siGENOME SMARTpool, 20 pmol in 71 mM NaCl), or negative control siRNA (Dharmacon, 20 pmol in 71 mM NaCl, see Supplementary Table S1 for sequence) using a 30-gauge needle. The footpad was then electroporated with 10 stimulations of 100 V/cm, 20-ms duration delivered at 1 Hz using subcutaneous gold-plated electrodes placed perpendicular to the long axis of the muscle, close to the proximal and distal tendons[40]. FDB muscles and fibers were used for experiments either 5-8 days after cDNA injection or boosted with a second round of siRNA electroporation on day 5-7 and then used for experiments 10-12 days after the initial electroporation.

Isolation of FDB muscle fibres

FDB muscle fibres were dissociated from FDB muscles from 4-6 month old male and female mice by enzymatic digestion in 0.1% collagenase A, 45 min at 37°C in Ringer's solution[40].

Bimolecular fluorescence complementation

Bimolecular fluorescence complementation **(**BiFC) is based on the association of two non-fluorescent fragments of yellow fluorescent protein (YFP) that fuse together to form a functional fluorophore when the fragments were located in close proximity (within 10 nm) to each other [28-30]. Thus, a putative interaction between two proteins can be examined by attaching complementary YFP fragments to the two proteins with YFP fluorescence used as a readout of the interaction. For these experiments, YFP was split into two fragments at amino acid 158. The N-terminal fragment of YFP (1-158) was fused to the C-terminus of cherry-tagged STIM1 and the C-terminal YFP fragment (159-238) was fused to the C-terminus of cherry-tagged Orai1 (Supplementary Fig. 2A). Cherry-STIM1-YFP1-158 and cherry-Orai1-YFP159-238 cDNAs were electroporated into mouse footpads at a 1:1 ratio. YFP fluorescence was monitored in cherry-expressing FDB fibers before and after store depletion. YFP and cherry were excited sequentially by 488 nm or 543 nm lasers, respectively, and fluorescence emission detected at 515/30 or 605/75 nm, respectively, with a Nikon Eclipse C1 Plus Confocal microscope (Nikon Instruments, Melville, NY, USA) using either SuperFluor 40x (1.3 NA) or 60x (1.4 NA) oil immersion objectives. Images were analyzed using AutoQuant software.

Mn^{2+} quench measurements

Acutely isolated single FDB fibers were loaded with 5 μM fura-2 AM for 1hr at 37° C in a Ca^{2+}-free rodent Ringer's solution containing (in mM): 145 NaCl, 5 KCl, 1 $MgCl_2$, 10 HEPES, 0.2 EGTA, pH 7.4. During fura-2 loading, unless otherwise stated, all fibres were simultaneously treated with a SERCA pump inhibitor cocktail consisting of 1 μM thapsigargin, 15 μM CPA and 30 μM *N*-benzyl-p-toluene sulfonamide (BTS), a skeletal muscle myosin inhibitor used to inhibit movement during electrical stimulation, in order to deplete SR Ca^{2+} stores, prevent Ca^{2+} reuptake, and activate SOCE. Store-depleted fibers were then plated on glass-bottom dishes, bathed in Ca^{2+}-free Ringer's and excited at 362 nm (isobestic point of fura-2) while emission was detected at 510 nm using a DeltaRam illumination system (Photon Technology, Birmingham, NJ). After obtaining an initial rate of fura-2 quench from ($R_{baseline}$), FDB fibers were then exposed to 0.5 mM $MnCl_2$ to access the rate of Mn^{2+} entry. The maximum rate of fura-2 quench in the presence of Mn^{2+} (R_{max}) was then obtained from the peak differential of the fura-2 emission trace during Mn^{2+} application. The rate of SOCE was calculated as $R_{SOCE}=R_{max}-R_{baseline}$ and expressed as dF/dt in counts/sec[12].

High Frequency tetanic stimulation of FDB fibres

Myoplasmic Ca^{2+} transient in FDB fibres during high frequency tetanic stimulation were monitored using mag-fluo-4[41] throughout the entire repetitive tetanic stimulation train (60 successive 500 ms, 50 Hz tetani every 2.5 s; Supplementary Fig. S2a, top). FDB fibres were

perfused with Ringer's solution in the presence or absence of Ca^{2+} influx blockers. Peak Ca^{2+} transient amplitude was measured at the end of each tetani and expressed as $(F_{max}-F_0)/F_0$ (Supplementary Fig. S2a). The integral of the Ca^{2+} transient decay following each tetanus was also calculated (Supplementary Fig. S2a). Average data were expressed as relative peak amplitudes and relative tail integrals to control for variability between cells.

Orai1 cloning and generation of dominant negative Orai1 mice

Total RNA was extracted from mouse spleen using TRIZOL reagent according to manufacturer instructions. Prior to reverse transcription, RNA was treated with DNAase I for 15 min at room temperature. RNA was then reverse-transcribed using Superscript III reverse transcriptase and oligo dTs. Murine WT Orai1 DNA was cloned using PCR and sequence-specific primers. A single amino acid dominant negative mutation in murine Orai1 (E108Q) was introduced using standard two-step site-directed mutagenesis. Three consecutive HA epitope (3×HA) sequences were similarly inserted in-frame at the extreme Orai1 C-terminus. The dnOrai1-3×HA construct was then cloned into a skeletal muscle specific transgene vector containing a human troponin I enhancer (hTnI USE), human skeletal muscle actin (*HSA*) promoter, and a BGH polyadenylation signal (pcDNA3.1(+)-hTnI-HSA-BGHpA (gift from Dr. Jeffery D. Molkentin)[42]. The vector was linearized and injected into pronuclei of fertilized mouse oocytes by the University of Rochester Medical Center (URMC) transgenic core facility. Founder lines exhibiting different levels of transgene incorporation were generated in a mixed background (B6SJL hybrid). Line 5 mice, exhibiting medium level of muscle-specific dnOrai1 protein expression (Fig. 3), were then backcrossed into C57Bl6 background. Genotyping was performed by PCR using the following primers:

Forward: 5’-CAAGTCCAGCTCGACACAGA-3’

Reverse: 5’-CTGCATAGTCCGGGACGTCATAGG-3’

Immunocytochemistry

Freshly isolated FDB fibres were fixed with 4% paraformaldehyde and labeled/co-labeled using different primary antibodies (Supplementary Table S2 for details) followed by appropriate Rhodamine/Alexa Fluor 488 conjugated secondary antibodies. Rhodamine and Alexa 488 were sequentially excited using 543 nm and 488 nm lasers, and detected at 605/75 nm and 515/30 nm, respectively, using a Nikon D-Eclipse C1 confocal microscope equipped with a 40×, NA1.3 oil-immersion objective. Images were averaged (n = 4) and deconvolved (2-D blind) for presentation.

Immunohistochemistry and H&E staining of TA muscle

Snap frozen tibialis anterior (TA) muscles from WT and dnOrai1 mice were cut into 10 μm thick sections and probed using a mouse monoclonal anti-dystrophin antibody (MANDRA1, abcam, 1:500). Sections were visualized using Alexa Fluor 488 anti-mouse antibody and imaged as described above (Immunocytochemistry). Fiber CSA was calculated using ImageJ software. Similar sections were alternatively stained using hematoxylin and eosin to assess muscle ultrastructure, specifically the presence of centrally nucleated fibres and fibrosis.

Electron microscopy (EM)

After sacrifice, EDL and FDB muscles were fixed in situ at room temperature and maintained in fixative (3.5% glutaraldehyde in 0.1 M NaCaCo buffer, pH 7.2) until use. Small portions of muscle were post-fixed, embedded, stained en-block, and sectioned[43]. Ultrathin sections (~50 nm), after staining in 4% uranyl acetate and lead citrate, were examined with a Morgagni Series 268D electron microscope (FEI Company, Brno, Czech Republic), equipped with Megaview III digital camera.

Western blot analysis

TA muscles were excised and homogenized in ice-cold RIPA buffer and centrifuged at 4°C, 16,000 × *g* for 15 min and supernatants were collected for analysis. Prepared sample were solubilised in standard Laemmli sample buffer prior to electrophoresis. Proteins were separated by SDS-PAGE, transferred to nitrocellulose membrane and immunostained with different primary antibodies followed by appropriate horseradish peroxidase-conjugated secondary antibodies (see Supplementary Table S2). Blots were visualised by enhanced chemiluminescence. Protein band densities were quantified using ImageJ software, using either GAPDH or α-actinin as loading controls. Full-length images of immunoblots are shown in Supplementary Figure S7.

Measurements of total SR Ca^{2+}

FDB fibres were loaded with 4 μM fura-2FF AM at room temperature for 30 min followed by a 30 min washout in dye free ringer solution. Total SR Ca^{2+} content was determined by fura2-FF fluorescence after local application of a Ca^{2+} release cocktail (ICE-10 μM ionomycin, 30 μM CPA, and 100 μM EGTA/0 Ca^{2+})[33].

Myosin heavy chain analysis

TA, EDL, soleus and FDB muscles from 4-6 month old male and female WT and dnOrai1 mice were homogenized on ice in a buffer containing (in mM) 20 Imidazole (pH 7.2), 150 KCl and 0.2 EDTA with protease inhibitors. Tissue homogenates were centrifuged at 4°C, 16,000 × *g* for 15 minutes. Pellets were resuspended in a buffer containing (in mM) 50 Tris-HCl (pH 7.4), 150 NaCl with protease inhibitors, snap frozen and stored at 80°C until use. Prior to analysis, prepared samples were diluted 1:1 in a sample buffer containing 0.16 M Tris-HCl (pH 6.8), 40% Glycerol, 4% SDS, 0.1 M DTT and 0.02% bromophenol blue, and solubilised at 95 °C for 5 min. Myosin heavy chain isoforms were separated using SDS-PAGE as described previously[44,45] with modifications. Electrophoresis were carried out using a Bio-Rad Mini Protean system, with resolving gels containing 8% acrylamide/bis (99:1), 35% Glycerol, 0.4% SDS, 0.2M Tris-HCl (pH 8.8), 0.1M Glycine, 0.1% APS, 0.05% TEMED and stacking gels containing 30% Glycerol, 4% acrylamide/bis (49:1), 0.4% SDS, 70 mM Tris-HCl (pH 6.7), 4 mM EDTA, 0.1% APS, 0.05% TEMED. 1.5 μg of protein was loaded in each lane. Gels were electrophoresed at 140V for 16-18 hrs at 4°C in running buffers containing: outer chamber, 0.05M Tris, 0.075M Glycine 0.05% SDS; inner chamber: 8x the concentration of outer chamber supplemented with 0.12% β-mercaptoethanol. After electrophoresis, protein bands were visualized by silver staining, photographed and relative composition of myosin heave chain isoforms were determined using ImageJ program.

In vitro muscle contraction assay

Muscle strength and fatigability were analyzed in EDL muscles using an ASI muscle contraction system (Aurora Scientific), equipped with a 300C-LR dual mode force transducer and a 701C stimulator. Mice were anaesthetized by intra-peritoneal injection of 100 mg/kg ketamine, 10 mg/kg xylazine, and 2 mg/kg acepromazine. EDL muscles were exposed after removing TA muscles. The proximal and distal tendons of EDL muscle were then tied using 4-0 surgical suture and EDL muscles were carefully excised and mounted between two platinum electrode plates while continuously perfused with oxygenated Ringer solution in the experimental chamber.[46] Muscle optimal length (L_o) was determined using a series of 1 Hz stimulation and set at the length that generates the maximal force. Stimulus output was set at 120% of the voltage that elicits maximal force. Muscles were first equilibrated using three 500 ms, 150 Hz tetani at 1 min intervals and then subjected to a force frequency, a single sustained high frequency tetanus (150 Hz, 2 sec) and/or a repetitive tetanic fatiguing (60 successive 50Hz, 500ms tetani) protocol. Muscle force was recorded using a Dynamic Muscle Control software and analysed using Clampfit 10.0 software. Muscle cross-sectional area and specific force were calculated as described previously[46].

In vivo fatigue assays

Rota-rod and treadmill running were used to assess the fatigability of 4-6 month old male and female WT and dnOrai1 mice during rigorous exercise. For rota-rod endurance task, mice were first acclimated to rota-rod running for 1 hour on a Rotamex-5 (Columbus Instruments) at 15 rpm for two consecutive days. On the following day, mice were placed on the rotarod at an initial speed of 15 rpm for 15 min. The speed was then increased by 1 rpm every 5 min for the following 30 min and then by 1 rpm every 15 min for the rest of the 2hr task. In the event of a fall, the fall was noted and the mouse was returned to the rota-rod. The number of cumulative falls over time during the task was recorded for each mouse. For treadmill (Columbus Instruments) experiments, mice were pre-trained for treadmill running 3 days before experiments, for 5 mins each day at a speed of 5 meter/minute (m/min) at a 15° incline. An acute exhaustion protocol was used for the treadmill task. After a 5 min warm up at 5 m/min at a 15° incline, treadmill speed was increased 1 m/min every minute up to 20 m/min and remained at the max speed for an additional 40 min. The entire task was 1 km in distance and 1 hour in duration. Continued running was encouraged by delivering brief (<1 sec) spirits of air on the mouse's backside using a Whoosh Duster™. The number of rests was recorded for each mouse. Finally, the number of cumulative falls (Rota-rod) or cumulative rests (treadmill, binned every 5 min) across multiple animals for each genotype were then averaged and plotted against the duration of task.

Data analysis

Results are expressed as mean ± s.e.m. with statistical significance determined using Student-*t* test for simple comparison and one-way ANOVA followed by *post- hoc* Student-Newman-Keuls test for multiple comparisons. $p<0.05$ were considered as statistically significant.

Supplementary Material

Refer to Web version on PubMed Central for supplementary material.

ACKNOWLEGMENTS

We thank Dr. Jeffery Molkentin for kindly providing the muscle-specific transgene vector used to generate the dnOrai1 mice, Dr. Veit Flockerzi for providing an anti-Orai1 antibody, Ryan Loy for help with video editing, and Linda Groom and Sara Geitner for providing excellent technical assistance. We also thank Dr. Thurman Wheeler for providing access to the mouse treadmill used in this study. This study was supported by an NIH grant (AR059646 to R.T.D.), the Academia Dei Lincea Fund (to L.W.L.), and a NSF Predoctoral Fellowship (to E.M.C.).

REFERENCES

1. Parekh AB. On the activation mechanism of store-operated calcium channels. Pflugers Arch. 2006; 453:303–311. [PubMed: 16944196]
2. Liou J, et al. STIM is a Ca^{2+} sensor essential for Ca^{2+}-store-depletion-triggered Ca^{2+} influx. Curr Biol. 2005; 15:1235–1241. [PubMed: 16005298]
3. Roos J, et al. STIM1, an essential and conserved component of store-operated Ca^{2+} channel function. J Cell Biol. 2005; 169:435–445. [PubMed: 15866891]
4. Zhang SL, et al. STIM1 is a Ca^{2+} sensor that activates CRAC channels and migrates from the Ca^{2+} store to the plasma membrane. Nature. 2005; 437:902–905. [PubMed: 16208375]
5. Feske S, et al. A mutation in Orai1 causes immune deficiency by abrogating CRAC channel function. Nature. 2006; 441:179–185. [PubMed: 16582901]
6. Vig M, et al. CRACM1 is a plasma membrane protein essential for store-operated Ca^{2+} entry. Science. 2006; 312:1220–1223. [PubMed: 16645049]
7. Feske S. ORAI1 and STIM1 deficiency in human and mice: roles of store-operated Ca^{2+} entry in the immune system and beyond. Immunol Rev. 2009; 231:189–209. [PubMed: 19754898]
8. Kurosaki T, Baba Y. Ca^{2+} signaling and STIM1. Prog Biophys Mol Biol. 2010; 103:51–58. [PubMed: 20226808]
9. Parekh AB, Putney JW Jr. Store-operated calcium channels. Physiol Rev. 2005; 85:757–810. [PubMed: 15788710]
10. Smyth JT, et al. Activation and regulation of store-operated calcium entry. J Cell Mol Med. 2010; 14:2337–2349. [PubMed: 20807283]
11. Li T, et al. STIM1-Ca^{2+} signaling is required for the hypertrophic growth of skeletal muscle in mice. Molecular and Cellular Biology. 2012; 32:3009–3017. [PubMed: 22645307]
12. Lyfenko AD, Dirksen RT. Differential dependence of store-operated and excitation-coupled Ca^{2+} entry in skeletal muscle on STIM1 and Orai1. J Physiol. 2008; 586:4815–4824. [PubMed: 18772199]
13. Stiber J, et al. STIM1 signalling controls store-operated calcium entry required for development and contractile function in skeletal muscle. Nat Cell Biol. 2008; 10:688–697. [PubMed: 18488020]
14. Yarotskyy V, Dirksen RT. Temperature and RyR1 regulate the activation rate of store-operated Ca^{2+} entry current in myotubes. Biophys J. 2012; 103:202–211. [PubMed: 22853897]
15. Darbellay B, Arnaudeau S, Bader CR, Konig S, Bernheim L. STIM1L is a new actin-binding splice variant involved in fast repetitive Ca^{2+} release. The Journal of Cell Biology. 2011; 194:335–346. [PubMed: 21788372]
16. Prakriya M, Lewis RS. Potentiation and inhibition of Ca^{2+} release-activated Ca^{2+} channels by 2-aminoethyldiphenyl borate (2-APB) occurs independently of IP(3) receptors. J Physiol. 2001; 536:3–19. [PubMed: 11579153]
17. Prakriya M, Lewis RS. Separation and characterization of currents through store-operated CRAC channels and Mg^{2+}-inhibited cation (MIC) channels. J Gen Physiol. 2002; 119:487–507. [PubMed: 11981025]
18. Kurebayashi N, Ogawa Y. Depletion of Ca^{2+} in the sarcoplasmic reticulum stimulates Ca^{2+} entry into mouse skeletal muscle fibres. J Physiol. 2001; 533:185–199. [PubMed: 11351027]

19. Pan Z, et al. Dysfunction of store-operated calcium channel in muscle cells lacking mg29. Nat Cell Biol. 2002; 4:379–383. [PubMed: 11988740]
20. Zhao X, et al. Enhanced resistance to fatigue and altered calcium handling properties of sarcalumenin knockout mice. Physiol Genomics. 2005; 23:72–78. [PubMed: 15998745]
21. Rosenberg P, et al. TRPC3 channels confer cellular memory of recent neuromuscular activity. Proc Natl Acad Sci U S A. 2004; 101:9387–9392. [PubMed: 15199180]
22. Darbellay B, et al. STIM1- and Orai1-dependent store-operated calcium entry regulates human myoblast differentiation. J Biol Chem. 2009; 284:5370–5380. [PubMed: 19088073]
23. Soboloff J, Rothberg BS, Madesh M, Gill DL. STIM proteins: dynamic calcium signal transducers. Nat Rev Mol Cell Biol. 2012; 13:549–565. [PubMed: 22914293]
24. Edwards JN, et al. Ultra-rapid activation and deactivation of store-operated Ca^{2+} entry in skeletal muscle. Cell Calcium. 2010; 47:458–467. [PubMed: 20434768]
25. Launikonis BS, Murphy RM, Edwards JN. Toward the roles of store-operated Ca^{2+} entry in skeletal muscle. Pflugers Arch. 2010; 460:813–823. [PubMed: 20577885]
26. Launikonis BS, Ríos E. Store-operated Ca^{2+} entry during intracellular Ca^{2+} release in mammalian skeletal muscle. The Journal of Physiology. 2007; 583:81–97. [PubMed: 17569733]
27. Dirksen RT. Checking your SOCCs and feet: the molecular mechanisms of Ca^{2+} entry in skeletal muscle. J Physiol. 2009; 587:3139–3147. [PubMed: 19406875]
28. Kerppola TK. Design and implementation of bimolecular fluorescence complementation (BiFC) assays for the visualization of protein interactions in living cells. Nat Protoc. 2006; 1:1278– 1286. [PubMed: 17406412]
29. Kerppola TK. Complementary methods for studies of protein interactions in living cells. Nat Methods. 2006; 3:969–971. [PubMed: 17117150]
30. Kerppola TK. Visualization of molecular interactions by fluorescence complementation. Nat Rev Mol Cell Biol. 2006; 7:449–456. [PubMed: 16625152]
31. Canato M, et al. Massive alterations of sarcoplasmic reticulum free calcium in skeletal muscle fibers lacking calsequestrin revealed by a genetically encoded probe. Proc Natl Acad Sci U S A. 2010; 107:22326–22331. [PubMed: 21135222]
32. Capote J, Bolanos P, Schuhmeier RP, Melzer W, Caputo C. Calcium transients in developing mouse skeletal muscle fibres. J Physiol. 2005; 564:451–464. [PubMed: 15731192]
33. Loy RE, et al. Muscle weakness in Ryr1I4895T/WT knock-in mice as a result of reduced ryanodine receptor Ca^{2+} ion permeation and release from the sarcoplasmic reticulum. J Gen Physiol. 2011; 137:43–57. [PubMed: 21149547]
34. Cheng KT, Liu X, Ong HL, Ambudkar IS. Functional requirement for Orai1 in store-operated TRPC1-STIM1 channels. J Biol Chem. 2008; 283:12935–12940. [PubMed: 18326500]
35. Zhao X, Moloughney JG, Zhang S, Komazaki S, Weisleder N. Orai1 mediates exacerbated Ca^{2+} entry in dystrophic skeletal muscle. PLoS ONE. 2012; 7:e49862. [PubMed: 23185465]
36. Edwards JN, et al. Upregulation of store-operated Ca^{2+} entry in dystrophic mdx mouse muscle. Am J Physiol Cell Physiol. 2010; 299:C42–50. [PubMed: 20427714]
37. Cully TR, Launikonis BS. Store-operated Ca^{2+} entry is not required for store refilling in skeletal muscle. Clin Exp Pharmacol Physiol. 2013; 40:338–344. [PubMed: 23517302]
38. Thornton AM, et al. Store-Operated Ca^{2+} Entry (SOCE) Contributes to Normal Skeletal Muscle Contractility in young but not in aged skeletal muscle. Aging (Albany NY). 2011
39. Duke AM, Hopkins PM, Calaghan SC, Halsall JP, Steele DS. Store-operated Ca^{2+} entry in malignant hyperthermia-susceptible human skeletal muscle. J Biol Chem. 2010; 285:25645–25653. [PubMed: 20566647]
40. Wei L, et al. Mitochondrial superoxide flashes: metabolic biomarkers of skeletal muscle activity and disease. FASEB J. 2011; 25:3068–3078. [PubMed: 21646399]
41. Rossi AE, Boncompagni S, Wei L, Protasi F, Dirksen RT. Differential impact of mitochondrial positioning on mitochondrial Ca^{2+} uptake and Ca^{2+} spark suppression in skeletal muscle. Am J Physiol Cell Physiol. 2011; 301:C1128–1139. [PubMed: 21849670]
42. Brennan KJ, Hardeman EC. Quantitative analysis of the human alpha-skeletal actin gene in transgenic mice. Journal of Biological Chemistry. 1993; 268:719–725. [PubMed: 7678010]

43. Boncompagni S, et al. Characterization and temporal development of cores in a mouse model of malignant hyperthermia. Proc Natl Acad Sci U S A. 2009

44. Talmadge RJ, Roy RR. Electrophoretic separation of rat skeletal muscle myosin heavy-chain isoforms. J Appl Physiol. 1993; 75:2337–2340. [PubMed: 8307894]

45. Mizunoya W, Wakamatsu J.-i. Tatsumi R, Ikeuchi Y. Protocol for high-resolution separation of rodent myosin heavy chain isoforms in a mini-gel electrophoresis system. Analytical Biochemistry. 2008; 377:111–113. [PubMed: 18358820]

46. Hakim, C.; Li, D.; Duan, D. Monitoring Murine Skeletal Muscle Function for Muscle Gene Therapy. In: Duan, D., editor. Muscle Gene Therapy. Vol. 709. Humana Press; 2011. p. 75-89.

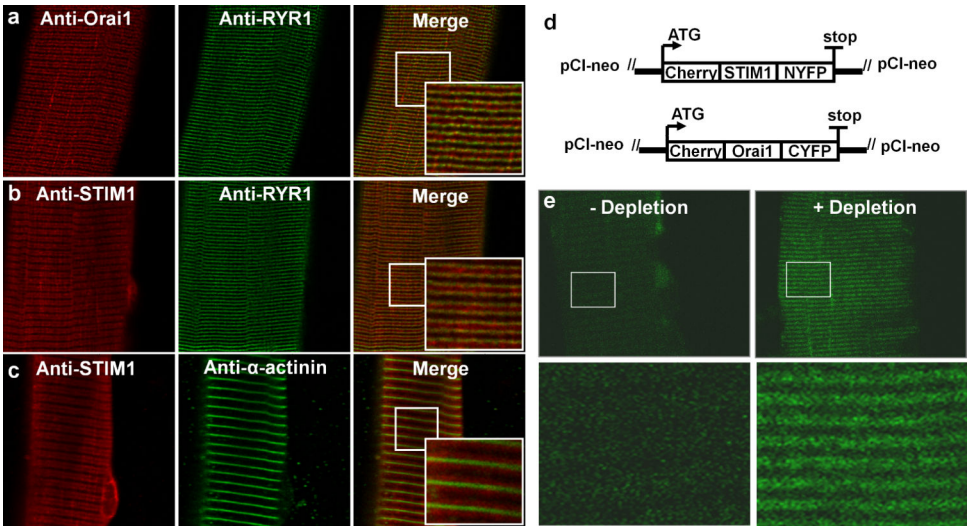

Figure 1. Co-localisation of endogenous STIM1 and Orai1 at the triad junction and formation of STIM1-Orai1 complexes upon store depletion

(a) Representative immunofluorescence images of endogenous Orai1 alone (left), RyR1 alone (middle), and overlay (right) in a FDB fibre from an adult WT mouse. (b) Representative immunofluorescence images of endogenous STIM1 alone (left), RyR1 alone (middle), and overlay (right) in a FDB fibre from an adult WT mouse. (c) Representative immunofluorescence images of endogenous STIM1 alone (left), α-actinin alone (middle), and overlay (right) in a FDB fibre from an adult WT mouse. Scale bars: 10 μm for low magnification images and 2 μm for high magnification images. (c) Schematic maps of split YFP constructs used in BiFC experiments. The N-terminal fragment of YFP (1-158) was fused to the C-terminus of cherry-tagged STIM1 (left) and the C-terminal YFP fragment (159-238) was fused to the C-terminus of cherry-tagged Orai1 (right). (d) (Top) Representative images of YFP fluorescence in FDB fibres expressing Cherry-STIM1-NYFP and Cherry-Orai1-CYFP before (left) after (right) TG-induced store depletion. Scale bars=10 μm. (Bottom) Higher magnification images in the boxed regions shown in the top panels. Scale bars=2 μm.

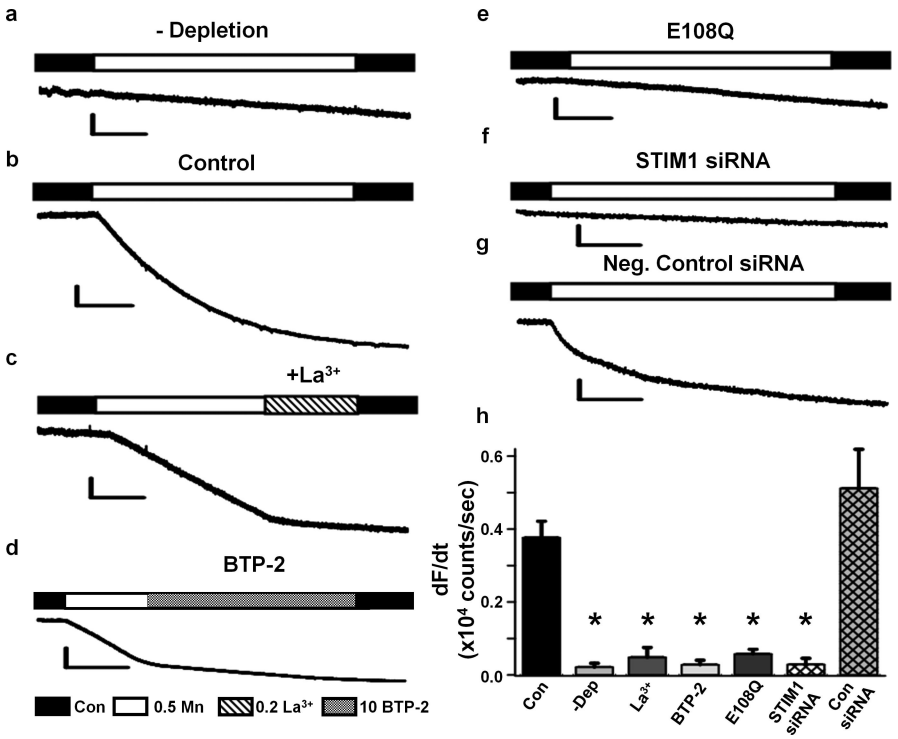

Figure 2. SOCE in adult skeletal muscle depends on STIM1-Orai1 coupling

(a) Representative Mn^{2+} quench trace in an adult FDB fibre in the absence of store depletion. (b-g) Representative Mn^{2+} quench traces in adult FDB fibres obtained following TG-induced store depletion in control (b), during addition of 200 μM La^{3+} (c), during addition of 10 μM BTP-2 (d), following expression of cherry-tagged E108Q (e), STIM1 siRNAs (f), or negative control siRNAs (g). (h) Average (±s.e.m.) maximum rate of Mn^{2+} quench in the absence of store depletion (-Dep, n=4) and following Tg-induced store depletion in control (Con, n=29), 200 μM La^{3+} (n=4), 10 μM BTP-2 (n=10), cherry-tagged E108Q expression (n=12), STIM1 siRNAs (n=8), and negative control siRNAs (n=9). *p<0.01 compared to control by ANOVA and *post-hoc* Student-Newman-Keuls test. Scale bars: horizontal: a-e =100 s, f-g = 50 s; vertical: a-e, 0.2×10^6 counts; f-g, 0.1×10^6 counts.

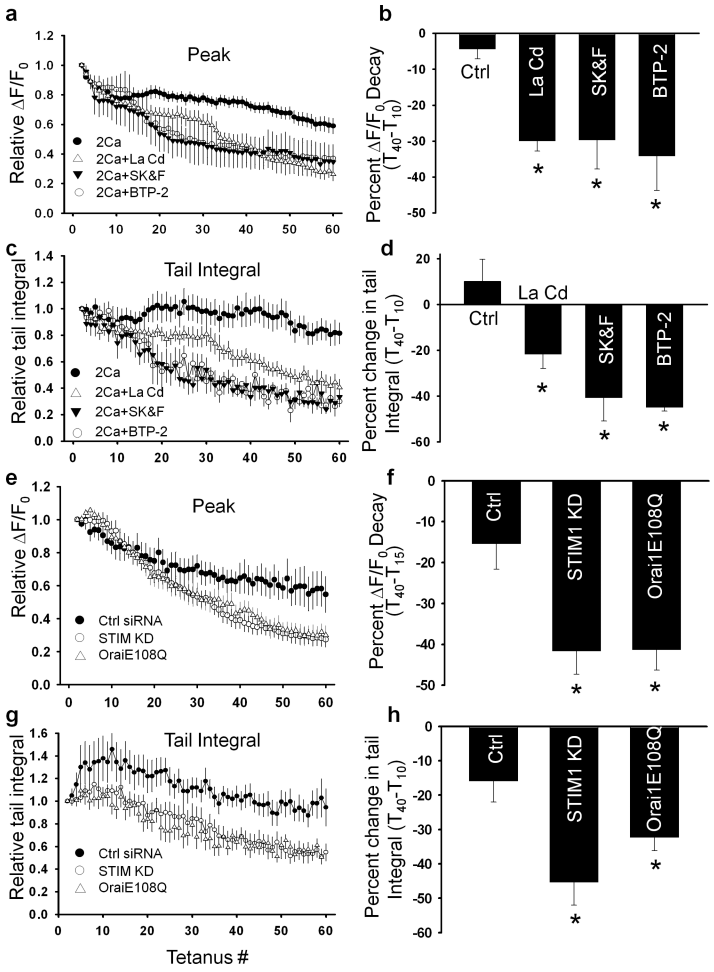

Figure 3. SOCE maintains Ca^{2+} transient amplitude during repetitive tetanic stimulation

(a) Average (±s.e.m.) peak Ca^{2+} transient amplitude during 60 consecutive tetanic stimuli (500 ms, at 50Hz, every 2.5 s) in control (2 Ca^{2+}, filled circles, n=14) or on the presence of 200 μM La^{3+} plus 500 μM Cd^{2+} (open triangles, n=15), 30 μM SK&F-96365 (inverted filled triangles, n=5) or 10 μM BTP-2 (open circles, n=6). (b) Average (±s.e.m.) percent reduction in peak Ca^{2+} transient amplitude from tetanus 10 to tetanus 40 ($[T_{40}\text{-}T_{10}]\times100$) in the absence and presence of blockers. (c) Average (±s.e.m.) relative Ca^{2+} transient tail integral after each tetani for the experiments in shown in a. (d) Average (±s.e.m.) percent change in peak Ca^{2+} transient decay ($[T_{40}\text{-}T_{10}]\times100$) for the experiments shown in a. (e) Average (±s.e.m.) peak Ca^{2+} transient amplitude during 60 consecutive tetanic stimuli (500 ms, at 50Hz, every 2.5 s) in FDB fibres treated with either negative control siRNA (Ctrl siRNA, filled circles, n=10), STIM1 targeted siRNA (STIM KD, open circles, n=18), or expressing cherry-tagged Orai1E108Q cDNA (open triangles, n=5). (f) Average (±s.e.m.) percent reduction in peak Ca^{2+} transient amplitude from tetanus 15 to tetanus 40 ($[T_{40}\text{-}T_{15}]\times100$) in FDB fibres treated with negative control siRNA or STIM1 targeted siRNA or Orai1E108Q cDNA (n=5) (g). Average (±s.e.m.) relative Ca^{2+} transient tail integral for the experiments shown in E. (h) Average (±s.e.m.) percent reduction in peak Ca^{2+} transient amplitude ($[T_{40}\text{-}T_{10}]\times100$) for the experiments shown in g. *p<0.05 compared to control by ANOVA and *post-hoc* Student-Newman-Keuls test.

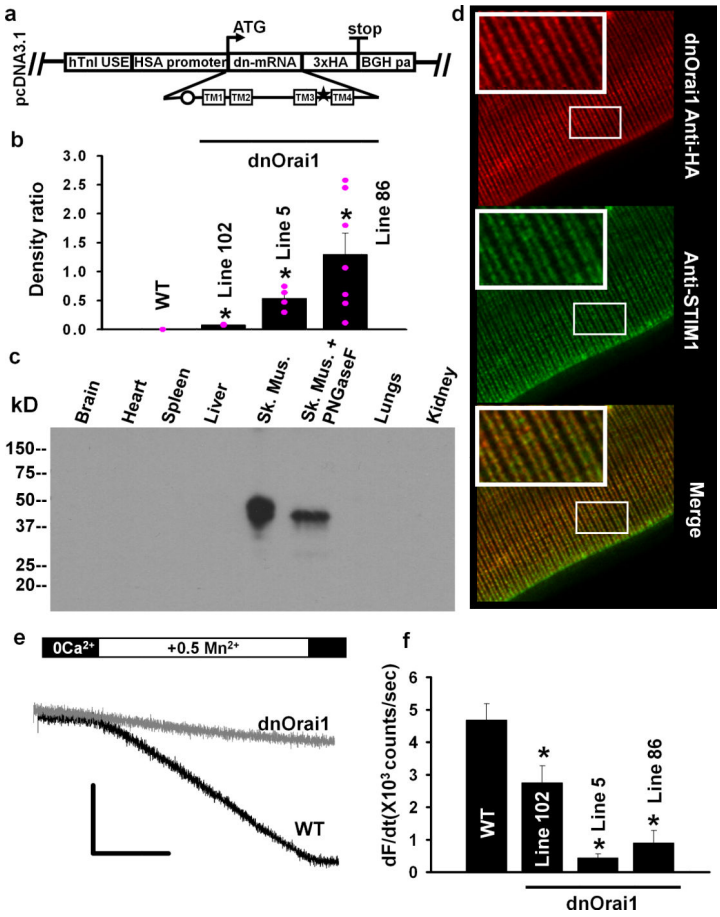

Figure 4. Generation of muscle-specific dnOrai1 transgenic mice

(a) Schematic representation of the transgene vector used to create multiple lines of muscle-specific dnOrai1 mice. The dominant negative E108Q point mutation and a C-terminal 3× HA epitope were engineered into a mouse Orai1 cDNA and then cloned into a transgene vector containing a human troponin I upstream enhancer (hTnIUSE), a human skeletal muscle actin (HSA) promoter, and a 3' bovine growth hormone polyadenylation (BGHpa) tail. (b) Relative HA-tagged dnOrai1 protein expression in TA muscles from WT (n=3) and dnOrai1 transgenic lines 102 (n=3), 5 (n=4), and 86 (n=7) probed by an anti-HA antibody using western blot analysis. HA immunoreactivity was normalized to SERCA. Pink filled circles (●) indicate the relative expression of dnOrai1 in every individual mouse analysed. *p<0.05 by ANOVA followed by Dunn's *posthoc* test. Line 5 mice exhibit uniform moderate transgene expression while line 86 mice exhibit high but more variable tansgene expression. (c) Western blot analysis with an anti-HA antibody showing skeletal muscle-specific expression of dnOrai1 protein in line 5 mice. (d) Imunonocytochemical labeling of dnOrai1 with anti-HA antibody (top), endogenous STIM1 (middle), and a merged image showing co-localisation of the two proteins in double-rows of striated fluorescence reflecting triad distribution (bottom). Scale bar =10 μm. (e) Representative Mn^{2+} quench traces in TG-treated FDB fibres obtained from wild type (WT) and line 86 dnOrai1 mice. Scale bars: horizontal, 100s, vertical, 4×10^5 counts. (f) Average (±s.e.m.) maximum rate of

Mn^{2+} quench in TG-treated FDB fibres from WT (n=9), line 102 (n=13), line 5 (n=15), and line 86 (n=7) dnOrai1 mice. *p<0.05 compared to WT by Student's t-test.

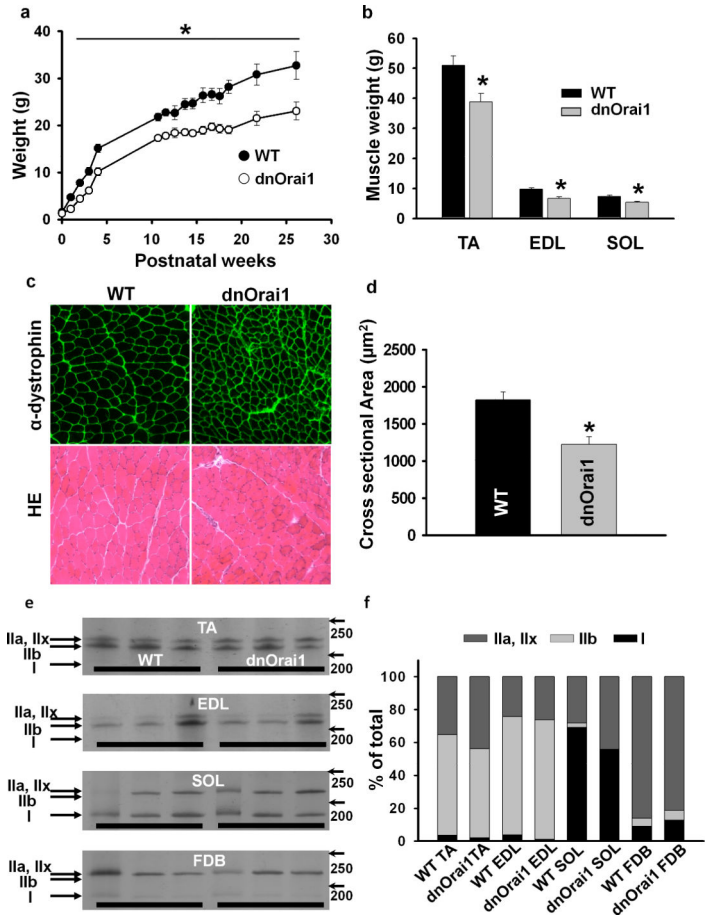

Figure 5. Reduced weight and fibre cross-sectional area in dnOrai1 transgenic mice

(a) Postnatal growth curves (birth to 6 months) obtained from line 5 mice showing a significant reduction in total body weight of muscle-specific dnOrai1 transgenic mice compared with WT littermate controls (n=5 female mice with both WT and dnOrai1). *p<0.01 compared to WT by Student's t-test. (b) Average (±s.e.m.) muscle weight of TA, EDL, and SOL in line 5 dnOrai1 transgenic mice (n=5 mice) compared to that of WT littermate controls (n=7 mice). *p<0.05 compared to corresponding WT control by Student's t-test. (c) Representative dystrophin immunostaining (top panel) and H&E images (bottom panel) of TA muscle cross sections from WT and line 5 dnOrai1 mice. Scale bars=100μm. (d) Average (±s.e.m.) fiber cross-sectional area calculated from dystrophin-stained TA muscle (as shown in c) from WT (n=4) and line 5 dnOrai1 mice (n=3). *p<0.05 by Student's t-test. (e) Representative silver-stained polyacrylamide gel images of myosin heavy chain analysis from TA, EDL SOL and FDB of three different WT and line 5 dnOrai1 mice. Molecular weight markers are indicated to the right of each gel. (f) Stacked bar graph showing average fast IIa, IIx, IIb and slow type I fibre composition in WT and line 5 dnOrai1 transgenic mice (n=3-5 for both WT and dnOrai1). No significant difference in fiber type composition was observed between WT and dnOrai1 mice.

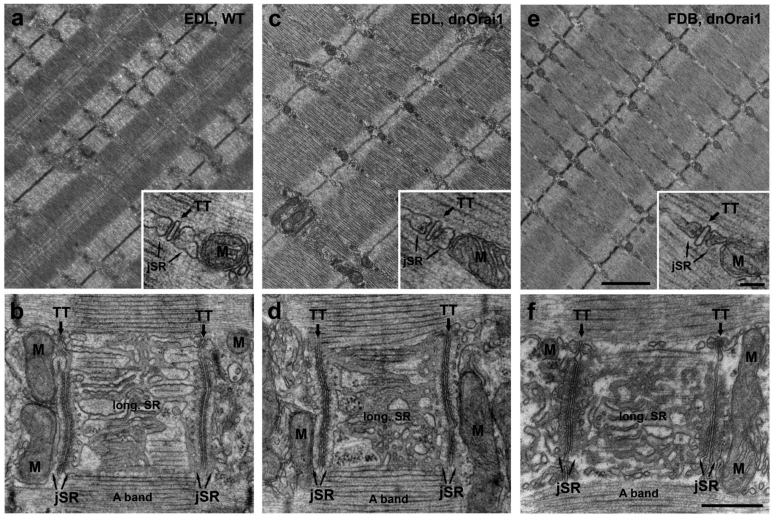

Figure 6. Preserved skeletal muscle ultrastructure in EDL and FDB muscle of line 5 dnOrai1 mice

Representative EM micrographs from WT EDL (a-b), line 5 dnOrai1 EDL (c-d), and line 5 dnOrai1 FDB (e-f), with all samples exhibiting similar ultrastructure. Sarcomeres of adjacent myofibrils are similarly well-aligned (a, c, and e), with triads and mitochondria closely associated (insets). Junctional SR (jSR) is closely associated with transverse tubules (TT) adjacent to the sarcomere I-A band transition, whereas longitudinal SR (long. SR) is placed at the A band (images are close to the surface of a myofibril) (b, d, and f). Mitochondria (M) are in close proximity of jSR/TT junctions (triads) on the side opposite to long. SR in fibres from both WT (b) and dnOrai1 (d,f) mice. Bars: a, c and e: 1 μm; b, d, and f: 0.5 μm; insets, 0.1 μm.

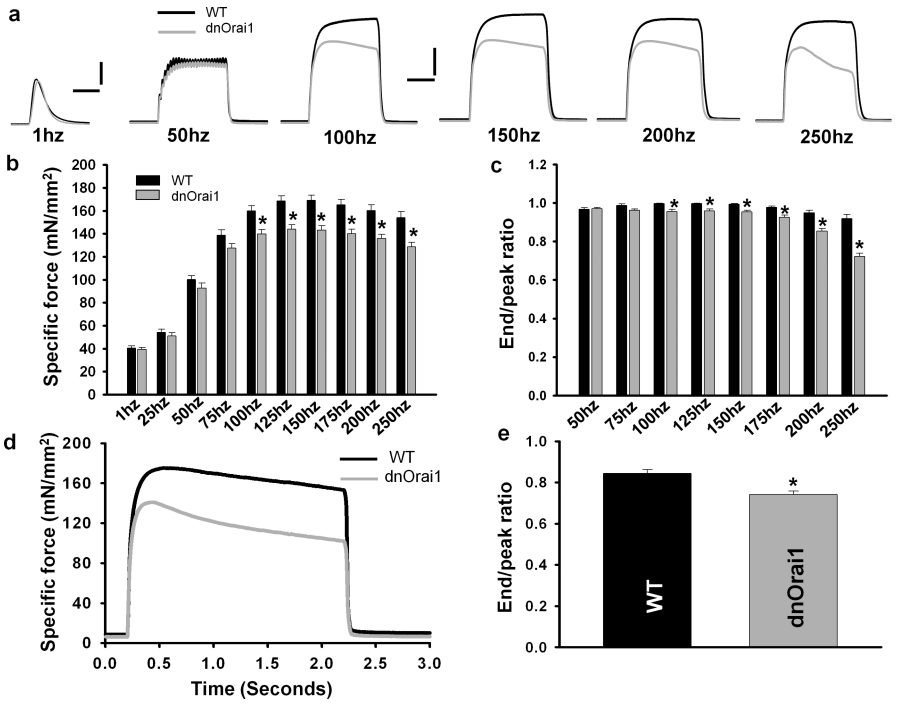

Figure 7. Altered maximum tetanic specific force and contractile decay in EDL muscles of dnOrai1 mice

(a) Representative superimposed contraction traces elicited at different stimulation frequencies (1, 50, 100, 150, 200, and 250 Hz) in EDL muscles from WT (black) and line 5 dnOrai1 (grey) mice. (b) Frequency dependence of average (±s.e.m.) specific force (mN/mm^2) in EDL muscles from WT (black, n=14) and line 5 dnOrai1 mice (grey, n=14). *p<0.01 compared to corresponding control by Student's t-test. (c) Frequency dependence of average (±s.e.m.) contractile decay (end/peak ratio) for EDL muscles from WT (black bars, n=14) and line 5 dnOrai1 (grey bars, n=14). *p<0.01 compared to corresponding control by Student's t-test. (d-e) Representative contractile traces (d) and average contractile decay (end/peak ratio, e) during a single 2 s, 150 Hz stimulation train in EDL muscles from WT (black, n=10) and line 5 dnOrai1 mice (grey, n=11). *p<0.01 compared to WT by Student's t-test. Scale bars: left, for twitch only, horizontal, 50ms; vertical $20mN/mm^2$; right, for tetani, horizontal, 200ms; vertical $50mN/mm^2$.

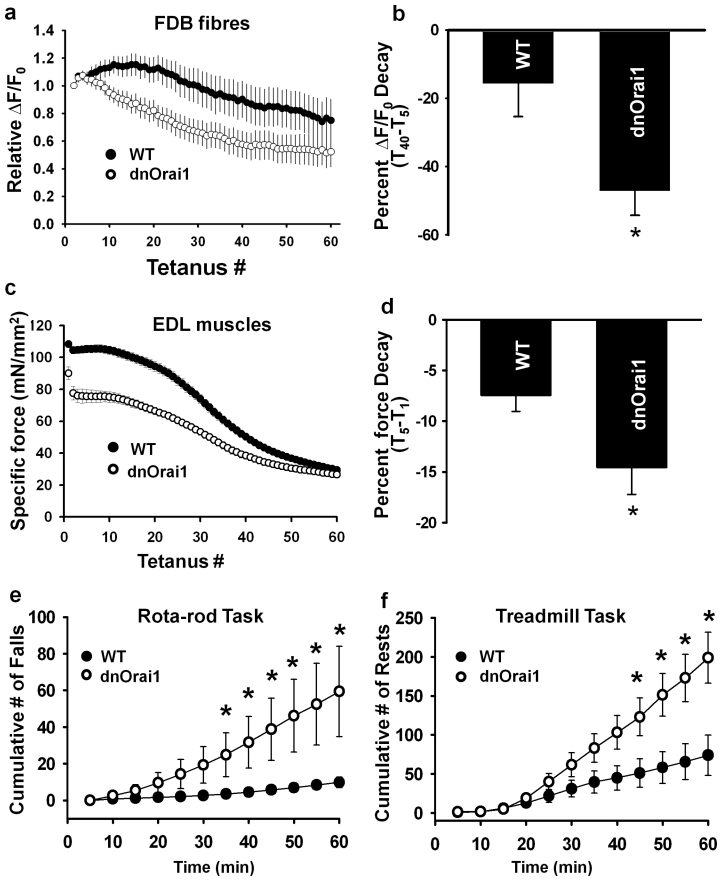

Figure 8. dnOrai mice exhibit increased susceptibility to fatigue

(a) Average (±s.e.m.) peak Ca^{2+} transient amplitude during 60 consecutive tetanic stimuli (500 ms, at 50Hz, every 2.5 s) in FDB fibres obtained from either WT (filled circles, n=11) or line 86 dnOrai1 transgenic mice (open circles, n=15). (b) Average (±s.e.m.) percent reduction in peak Ca^{2+} transient amplitude from tetanus 5 to tetanus 40 ($[T_{40}\text{-}T_5]\times100$) for the experiments shown in a. *p<0.05 by Student's t-test. (c) Average (±s.e.m.) peak specific force during 60 consecutive tetanic stimuli (500 ms, at 50Hz, every 2.5 s) in EDL muscles from WT (filled circles, n=8 muscles from 4 mice) or line 5 dnOrai1 mice (open circles, n=8 muscles from 5 mice). (d) Average (±s.e.m.) percent force decay during the first five successive tetani ($100\times[T_5\text{-}T_1]/T_1$) for the experiments shown in c. *p<0.05 by Student's t-test. (e) Average (±s.e.m.) cumulative number of falls during 1 hr Roto-Rod endurance task in 4 month old adult WT (n=11) and line 5 dnOrai1 (n=9) mice (see Methods). *p<0.05 by Student's t-test. (f) Average (±s.e.m.) cumulative number of rests (i.e. all four paws off the treadmill) observed during 1 kilometre treadmill run in 4 month old adult WT (n=6) and line 5 dnOrai1 (n=5) mice (see Methods). *p<0.05 by Student's t-test. The phenotypes (absence of SOCE, reduced body and muscle weight, increased fatigue, reduced treadmill running) of line 5 mice on the mixed background (B6SJL hybrid) was the same as that observed for line 5 mice following backcross onto a congenic C57Bl6 background.